Geophysical Research Letters

RESEARCH LETTER
10.1029/2020GL089026

Magnetic Field Imaging of Salt Structures at Nordkapp Basin, Barents Sea

V. Paoletti[1], M. Milano[2], J. Baniamerian[3,4], and M. Fedi[1]

[1]Department of Earth, Environment and Resources Science, University of Naples Federico II, Naples, Italy, [2]Institute of Marine Sciences - National Research Council (ISMAR-CNR), Naples, Italy, [3]Dipartimento di Matematica e Fisica, Università degli Studi Roma Tre, Rome, Italy, [4]Department of Earth Sciences, College of Sciences and Modern Technologies, Graduate University of Advanced Technology, Kerman, Iran

Key Points:
- We interpret the magnetic field of the Nordkapp Basin by a multiscale approach
- Imaging methods applied to magnetic data can well identify the top, bottom, and shape of saline structures
- High-resolution aeromagnetic surveys are a valid and low-cost tool for mapping diapirism where other methods are not entirely effective

Correspondence to:
M. Milano,
maurizio.milano@unina.it

Citation:
Paoletti, V., Milano, M., Baniamerian, J., & Fedi, M. (2020). Magnetic field imaging of salt structures at Nordkapp Basin, Barents Sea. *Geophysical Research Letters*, *47*, e2020GL089026. https://doi.org/10.1029/2020GL089026

Received 4 JUN 2020
Accepted 26 AUG 2020
Accepted article online 30 AUG 2020

Abstract We show that high-resolution aeromagnetic surveys, although rarely employed in the research of salt structures, may be an effective and low-cost tool for mapping diapirism. A multiscale analysis of a high-resolution magnetic data set at Nordkapp Basin in the Barents Sea, allows a clear reconstruction of the main salt diapirs of the basin using Multiridge and Compact Depth from Extreme Points methods. We provide a 3-D model of the diapirs extended from 500 to 4,000 m below sea level, characterized by a general low magnetization contrast no larger than −0.08 A/m. The 3-D model is consistent with the salt top depth estimated by 2-D seismics, with borehole data and with the 2-D gravity model of the Uranus diapir. Our imaging shows the capability of the magnetic method that gives new and comprehensive pictures of salt diapirism.

1. Introduction

Hydrocarbon exploration requires a detailed image of the salt domes using geophysical techniques. Seismic reflection, gravity, and well data are commonly used to investigate the structure and tectonic evolution of evaporite basins (e.g., Barde et al., 2002; Davison et al., 2000; Gernigon et al., 2014; George et al., 2017; Gudlaugsson et al., 1998; Henriksen & Vorren, 1996; Mattos et al., 2016; Rowan & Vedenville, 2006). The reason is the large contrast in the physical properties of the evaporites (high seismic velocities and low densities) with respect to the overlying and surrounding sedimentary materials (e.g., Choi et al., 2011; Hayward et al., 2014).

Nevertheless, in some cases seismic imaging of salt diapirs has given rise to considerable problems in defining the geometries of salt flanks and subsalt reflectors, as the well-studied Nordkapp Basin in the Barents Sea demonstrates (e.g., Koyi et al., 1993; Nilsen et al., 1995; Xu et al., 2020). The uncertainty derives from seismic imaging distortion around the salt diapir area that makes the creation of a velocity model difficult. This is due to the large contrast of acoustic impedance between salt bodies and surrounding rocks and poor illumination, besides free-surface and internal multiples. The main difficulties are especially in mapping the salt base and flanks.

Other types of geophysical methods, such as magnetic and gravity techniques, can give important contributions to the interpretation and modeling of the whole salt structures, provided that data are at high resolution (e.g., Fichler et al., 2007; Geletti et al., 2014; Gernigon et al., 2011; Olesen et al., 2010; Stadtler et al., 2014). In addition, magnetic methods have low costs compared to seismic methods. Bain et al. (1993) and Saad (1993) suggest that magnetic anomalies identify the top and edges of the source in greater detail, whereas gravimetric anomalies are representative of the entire source and centered above it. The authors infer that the offset observed between the magnetic and gravimetric anomalies above diapirs, is due to the asymmetry of the shallower portion of the diapir that mainly influences magnetic data. Backé et al. (2010) note this offset may vary and be complicated by density variations within the evaporites.

Tilted sedimentary structures with low magnetic susceptibilities may produce detectable short-wavelength magnetic anomalies (Nabighian et al., 2005). Salt diapirs have small, low-amplitude, negative subcircular signatures located in correspondence with the shallow sedimentary layers deformed by salt during diapirism phenomena. The use of magnetic data for mapping salt structures is most effective when the salt lies

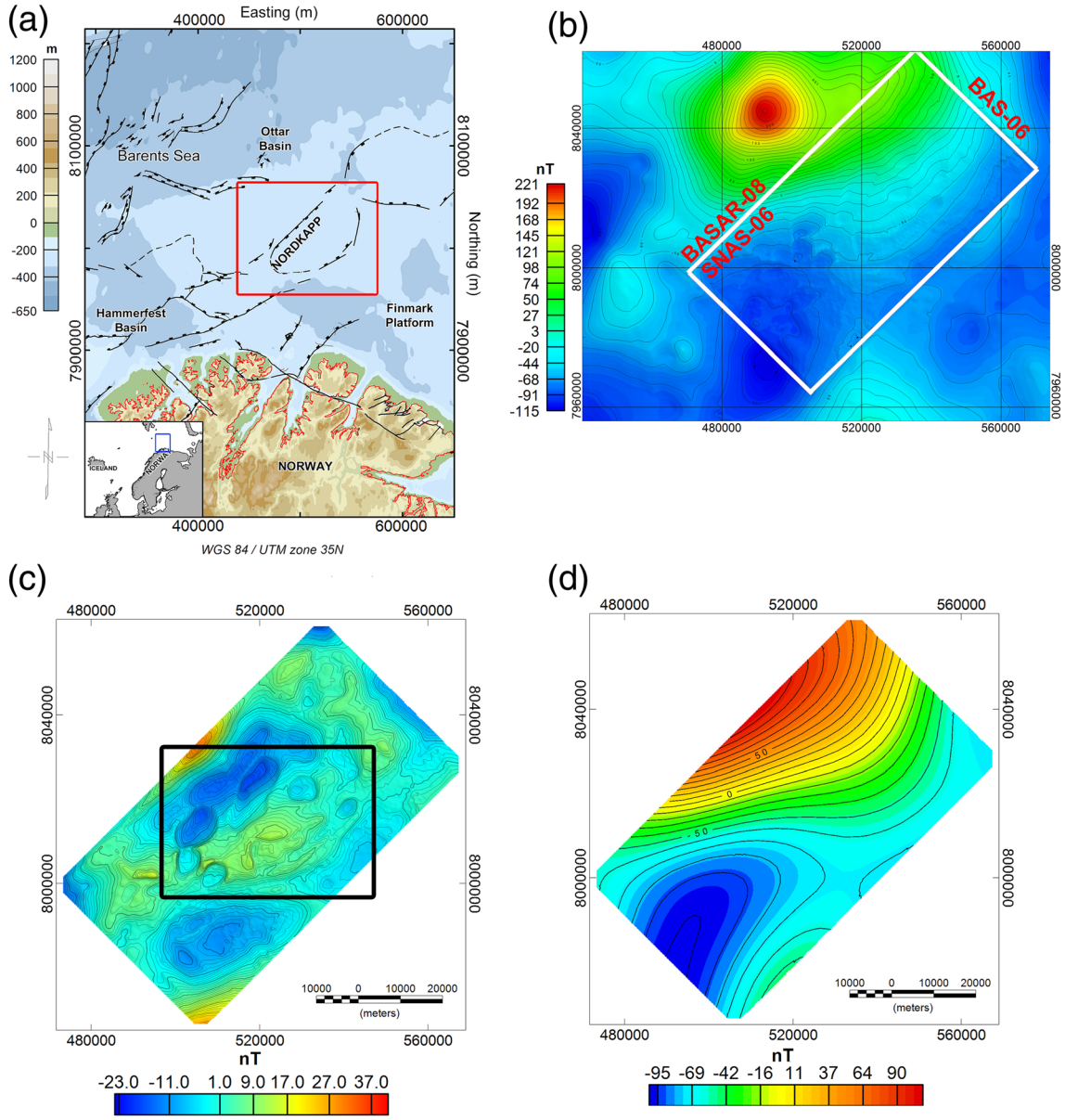

Figure 1. (a) The Nordkapp Basin in the southwestern Barents Sea. Structural lineaments (black lines) are from Bugge et al. (2002). The red box encloses the data sets shown in plot (b). Coastline in red; (b) high-resolution aeromagnetic data obtained by merging the BAS-06, BASAR-08, and SNAS-06 data sets (see text for details); (c) zoom of the data obtained after a filtering process involving high-pass with cutoff wavelength of 51 km and low-pass with cutoff wavelength of 1.5 km. The black box is the area of the CDEXP analysis (Figures 3 and 4); (d) zoom of the residual data after high-pass and low-pass filtering.

shallower than ~2–3 km, considering the small susceptibility contrast between salt and sediments (Gernigon et al., 2011).

In this paper, we study the anomalies of the Nordkapp Basin, a narrow fault-controlled graben of the western Barents Sea characterized by salt tectonics (Figure 1a). As the geology of the area is controlled by the complex interplay between salt movement and sedimentation (e.g., Henriksen & Vorren, 1996), a geophysical characterization of the salt structures of the graben is crucial for understanding the nature and tectonic of this sedimentary basin (e.g., Koehl et al., 2018; Rojo & Escalona, 2018).

We use multiscale methods to interpret the high-resolution magnetic data reported in Gernigon et al. (2011, 2014). More specifically, we infer the source type and depth using multiridge analysis of a multiscale data set (e.g., Fedi et al., 2009; Milano et al., 2016) and we retrieve the sources' actual geometry and magnetization

contrast using iterative imaging methods (Baniamerian et al., 2016; Liu et al., 2020) inherently based on the DEXP transformation (Fedi, 2007). Such methods are straightforward and have been effectively employed in several studies (e.g., Fedi & Pilkington, 2012; Fedi et al., 2018; Paoletti et al., 2016, 2019).

2. Geological and Geophysical Framework

The Nordkapp Basin (Figure 1a), along with other N-S to NE-SW trending basins, formed during a regional rift episode that affected the Barents Sea, Bjørnøya, and Svalbard from Late Devonian to Early Carboniferous (Bugge et al., 2002). The Nordkapp Basin is about 300 km long and 30–80 km wide and has a general NE-SW trend and an E-W orientation in its eastern part. The Barents Sea covers an intracratonic basin with Devonian to Quaternary sediments over a basement of Caledonian and pre-Caledonian rocks. The geological history and tectonic framework of the area are described in several publications (e.g., Bugge et al., 2002; Gabrielsen et al., 1990; Gernigon et al., 2014; Faleide et al., 1984; Nilsen et al., 1995; Rønnevik & Jacobsen, 1984; Vorren et al., 1991). Here we give only a summary focusing on the Nordkapp Basin. The basin is defined at base Cretaceous level (Gabrielsen et al., 1990) and is characterized by several diapirs and pillow-like salt structures along the basin margins, piercing to Quaternary level. Salt tectonics is believed to have started in the early Triassic during basement-involved regional extension and was reactivated in Tertiary time (e.g., Nilsen et al., 1995). Salt diapirism highly affected the early Tertiary sedimentation and was characterized by short periods of diapiric growth, commonly corresponding to regional tectonic phases (Nilsen et al., 1995). Thus, the evaluation of the interplay between salt movement and sedimentation is significant in inferring the early Tertiary evolution of the basin. According to most authors, salt rise was due to buoyancy and density contrast, whereas Nilsen et al. (1995) related the last salt diapirism to mid-Tertiary compression that led to squeezed and folded salt geometries (Bugge et al., 2002). The basin was then uplifted and eroded in Plio-Pleistocene times leading to the formation of subcropping salt features (Bugge et al., 2002). The Tertiary diapirism and Late Tertiary erosion exposed outcrops of Mesozoic rocks around salt diapirs below the Base Quaternary unconformity. The area was subsequently subsided and overlain by a cover (no thicker than 40 m) of Quaternary sediments bathymetry (e.g., Johansen et al., 1992).

Most sedimentary rocks do not contain significant amounts of magnetite or other magnetic minerals, so these rocks are low magnetic when compared with basement rocks. Nevertheless, subcropping, tilted/folded sedimentary structures with low magnetic susceptibilities may generate measurable short-wavelength magnetic anomalies (Nabighian et al., 2005). According to Lauritsen et al. (2007), Mørk et al. (2002) and Stadtler et al. (2014), the mean susceptibilities of sedimentary rocks surrounding the salt diapirs at Nordkapp Basin range between 100 and 2,000 $\times 10^{-6}$ SI units (8–160 $\times 10^{-6}$ cgs units), with an average value of 300 $\times 10^{-6}$ SI units (24 $\times 10^{-6}$ cgs units). Diapirs are slightly diamagnetic, or virtually non-magnetic, so their susceptibility can be considered negligible (Gernigon et al., 2011). Regarding magnetic remanence of the mid-Norwegian margin sedimentary rocks, Mørk et al. (2002) have observed that the magnetic anomalies of sedimentary rocks in the basin are only related to induced magnetism. Thus, considering an induction field of ~54,000 nT, the contrast rock/salt due only to induced magnetization is expected to be 0.005–0.09 A/m.

The Nordkapp Basin is characterized by a regional gravity low, edged by gravity highs related to major fault zones (Nilsen et al., 1995). In the southern basin, recent high-resolution aeromagnetic data acquired by the Norwegian Survey of Geology (SNAS-06, BAS-06, and BASAR-08; Gernigon et al., 2011, 2014) highlight several subcircular structures. Several magnetic signatures match with local gravity lows and are placed over the main salt structures highlighted by seismic-reflection data (e.g., Nilsen et al., 1995). A Cesium magnetometer flying at a ~230 m altitude above sea level (a.s.l.) over survey lines spaced 500 m acquired the high-resolution SNAS-06 data. The lower-resolution BAS-06 and BASAR-08 surveys were flown at the same altitude of the SNAS-06 survey, but with survey lines spaced 2 km.

The average water depth at the basin is ~300 m and most of the salt diapirs reach close to the seabed. Gernigon et al. (2011) and Stadtler et al. (2014) interpret the low-amplitude anomalies of the area lithologic as due to negative contrasts between sedimentary layers and salt diapirs at shallow- to intermediate-depth.

3. Multiridge Analysis of the Nordkapp Diapirs

Before performing multiridge analysis, we merged the SNAS-06, BAS-06, and BASAR-08 data sets by using the *Oasis Montaj GridKnit* function with a 200 m spacing. The amplitude variations associated with the diapirs are subtle and just above noise level (Figure 1b), with an amplitude <5 nT where the diapirs reach the sea bottom. To highlight the short-wavelengths salt-related signatures, we high-pass filtered the data with a 51 km cutoff wavelength; this wavelength showed to be the most suitable for removing the larger/deeper sources-related signal while leaving the salt-related signatures mostly untouched. Furthermore, we removed the high-frequency noise through a low-pass filter with a 1.5 km cutoff wavelength. The results clearly show subcircular, short wavelengths and subtle anomalies associated with the salt diapirs (Figure 1c).

We infer the depth to the sources using the multiridge geometric method, which considers the extreme points of the field and its *n*-order spatial derivatives at different altitudes and employs geometric criteria to find the source positions (Fedi et al., 2009). More specifically, the "ridges" (lines defined by the position of the extreme points of the field at different altitudes) are extrapolated into the source region and intersect each other at singular points corresponding to the sources. This method has the advantage of acting as a band-pass filter (Florio et al., 2009). The use of differentiation and upward continuation has indeed the contrasting effects of enhancing and reducing the high-frequency noise. Thus, the anomalies will result relatively smooth and isolated, even in the case of high differentiation orders and continuation altitudes.

For our study, we continued the data of Figure 1b) up to 3,000 m a.s.l. with a continuation step of 100 m, by using the classical convolution integral of the level-to-level upward continuation (e.g., Mastellone et al., 2014):

$$U(x,y,z)=\frac{1}{2\pi}\int_S U(\xi,\eta,0)\frac{z}{\left[(x-\xi)^2+(y-\eta)^2+z^2\right]^{3/2}}\mathrm{d}\xi\mathrm{d}\eta \tag{1}$$

where $U(x,y,z)$ is the potential field upward continued to the altitude z, $U(\xi,\eta,0)$ is the potential field at level $z = 0$ and $z/[(x-\xi)^2+(y-\eta)^2+z^2]^{3/2}$ is the upward continuation operator. To reduce upward-continuation errors and create a reliable 3-D data set for multiscale analysis, it is necessary to avoid aliasing from circular convolution and extrapolate the field to be continued on a larger area (Baniamerian et al., 2017; Fedi et al., 2012). We used the *maximum entropy extension algorithm* yielding the most accurate upward continued fields (with respect to other extrapolation algorithms). To get enough resolution to our study, we analyzed the third-order vertical derivative of the field (Figure 2), computed by the *integrated second vertical derivative* (ISVD) algorithm (Fedi & Florio, 2001) that gives more stable results than the usual Fourier method. We computed the horizontal derivatives of the field in the space domain by the finite difference method.

Then, we selected two profiles P1 and P2 crossing the salt structures signatures. The depths-to-the-sources resulting from the intersection of the extrapolated ridges in the underground are 750–1,200 m below sea level.

The data acquisition level is ~230 m, the depth of the seabed in the area is around 300 m below sea level (b.s.l.), and the quaternary coverage does not exceed 40 m of thickness below the bathymetry (e.g., Johansen et al., 1992). Thus, we locate sources at a minimum depth of about ~520 m b.s.l., corresponding to ~220 m with respect to the bathymetry and to about ~180 m with respect to the Quaternary discontinuity. From stratigraphic studies conducted in the region, we know that the Tertiary cover is practically eroded away and at the minimum estimated depth for the sources (about 440 m b.s.l.) there are units from the Lower Cretaceous (Johansen et al., 1992). This result confirms that the magnetic effects generated by the contact of saline diapirs with the Cretaceous layers, that contain ferrous minerals (siderite), are predominant when compared with those generated by discontinuities in other layers with low magnetic susceptibility (Fichler et al., 2007).

After selecting one or more ridges, we estimated the structural index N, which is related to the source shape (fault: $N = 0$, sill/dyke: $N = 1$, cylinder: $N = 2$, sphere: $N = 3$), through the *scaling function analysis* (Fedi, 2007; Florio et al., 2009):

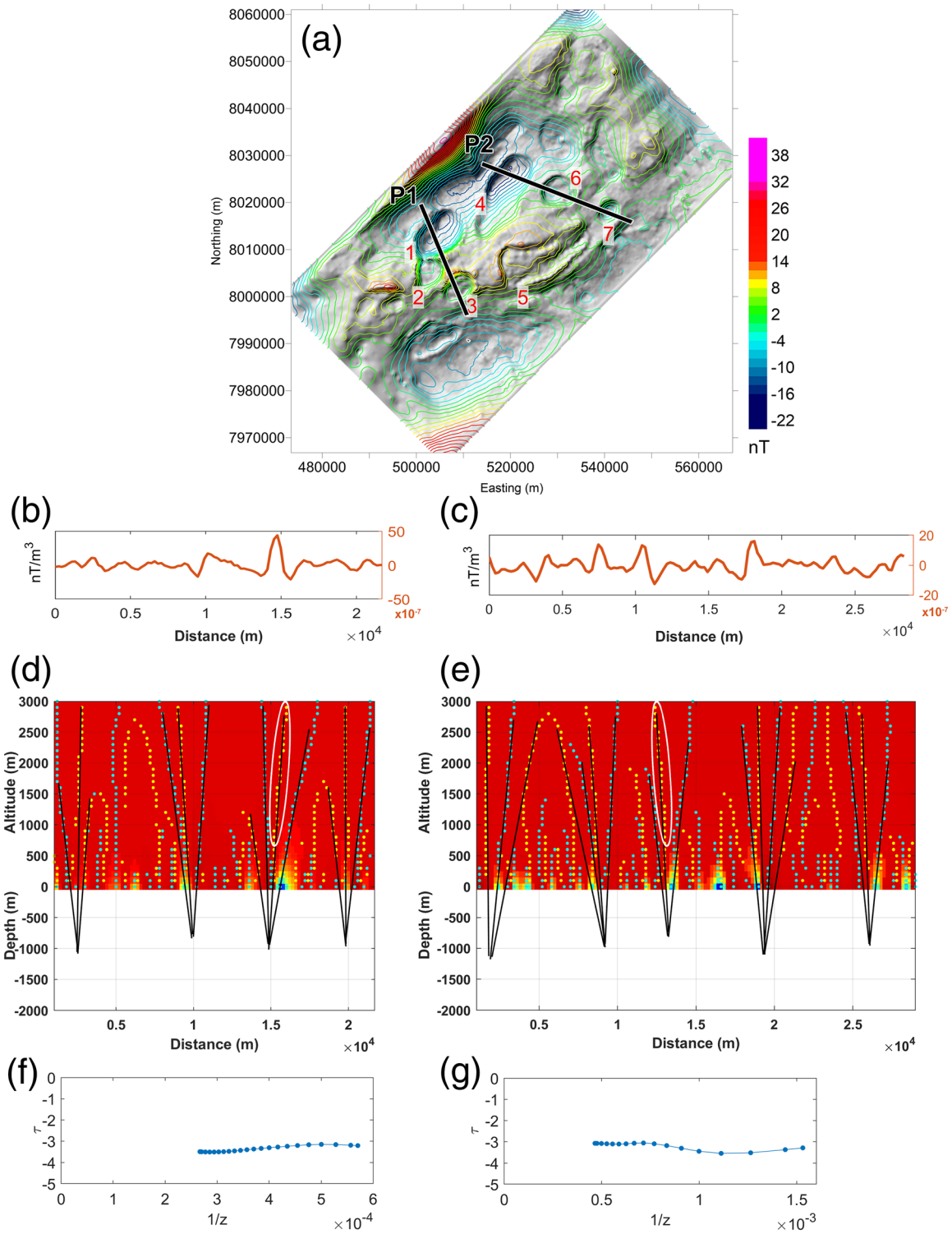

Figure 2. Multiridge analysis of the magnetic field along the two profiles P1 and P2: (a) Shaded relief image of the data of Figure 1b. The black lines are profiles P1 and P2; red numbers point out the seven studied diapirs; (b, c) third-order vertical derivative of the analyzed field at the measurement altitude along profiles P1 and P2; (d, e) multiridge plots along P1 and P2. Light blue dots in plots are the maxima of the vertical derivative of the field, yellow dots are the maxima of the horizontal derivative of the field, and black lines join the ridges and extrapolate them from the measurement plane into the source position. The resulting depths of the structures are of 750–1,200 m b.s.l. We recall that an average value of 230 m (magnetometer height) should be subtracted from these resulting depths. The white ellipses show the ridges selected for evaluating N; (f, g) estimation of N by the *scaling function* analysis for profiles P1 and P2. The intercept represents the value of $N + q$ (the differentiation order, $q = 3$ in this case), yielding to values of N ranging from 0.5 to 0.7, which may refer to an irregular morphology of the salt top.

$$\tau = \frac{\partial \log(f)}{\partial \log(z)} = \frac{nz}{z - z_0} \tag{2}$$

where τ is the scaling function, f is the analyzed field, z_0 is the depth to the source, z is the altitude, n is the homogeneity degree and

$$N = -n + q \; n<0 \tag{3}$$

with q being the field differentiation order.

Therefore, the study of the scaling function of gravity and magnetic fields allows retrieving the source depth and the structural index through an analysis along ridges. Simple idealized sources have integer structural indices, but in real-world cases, the estimated N is often not an integer and may vary with the distance of observation. A general theory on fractional n and N is described in Fedi et al. (2015). The intercept of the scaling function τ versus the reciprocal of the altitude $1/z$ yields an estimate of n from which we can easily compute the structural index N (Equation 3). When adopting the right depth to the source, the scaling function curve becomes flat and may be easily interpreted. In our analysis (Figure 2) we estimate a structural index near to 0.7, which may be associated to an irregular morphology of the salt top.

4. Imaging of Magnetic Data by Compact DEXP Method

We investigate the depth, shape and magnetization contrast of the Nordkapp salt structures by the Compact DEXP method (Liu et al., 2020). It is a multiscale iterative imaging method based on an upgrade of the DEXP method (Fedi, 2007) and Compact DEXP (CDEXP) approach (Baniamerian et al., 2016). DEXP transformation scales the upward continued field by a power law whose exponent depends on the source's structural index N (Fedi et al., 2010):

$$\Omega^{(q)}(x, y, h_i) = h_i^{\left(\frac{q+N}{2}\right)} \frac{\partial^q f(x, y, z)}{\partial z^q}\bigg|_{z=z_i} \qquad i = 1, \cdots, L. \tag{4}$$

where $\Omega^{(q)}$ is the DEXP transformation of the qth order vertical derivative of the field, x, y, z are the coordinates of the position vector, f is the potential field and $h_i = |z_i|$ is the ith depth level that corresponds to the ith altitude.

The method can be applied to gravity and magnetic fields and to their vertical or horizontal derivatives of any order as well, so reducing the interference effects related to close-by sources. This is due to the stability of upward continuation with respect to the high-frequency noise.

The DEXP transformation defined by Equation 4 provides an approximate and smooth image of the subsurface sources (Fedi & Pilkington, 2012). Ω can be simply converted into the causative source-physical property (g/cm^3 or A/m) through a constant, k, having adequate physical dimensions. k can be estimated by a linear regression of the observed field versus the field computed from DEXP image with a unit density/magnetization (Baniamerian et al., 2016):

$$m(x, y, h_i) = k \; \Omega(x, y, h_i) \tag{5}$$

where m is the source property (mass density/magnetic susceptibility) estimated directly from DEXP transformed field. This approach can be implemented iteratively to improve the obtained image from DEXP transformation itself. To this purpose, first, the subsurface space is divided into an array of cells, each cell being assigned the physical property obtained from converting the corresponding value of the DEXP image by Equation 4. The recovered source distribution provides a smooth image of the subsurface sources, and the corresponding predicted data may not well fit the measured data. Therefore, such a model needs to be improved to reconstruct a geologically feasible distribution of source. This can be achieved by implementing a compacting function, based on the estimated model at the previous iteration (Baniamerian et al., 2016; Liu et al., 2020; Pilkington, 2009):

$$\mathbf{W}_i = 1 + \frac{\boldsymbol{\rho}_{i-1}^2}{\sigma^2} \tag{6}$$

where $\boldsymbol{\rho}_i$ is the density/magnetization model obtained at the $(i-1)$th iteration, and σ is a positive-value parameter with the same dimension as physical property that controls the degree of compactness or

focusing. An appropriate value of σ is usually chosen on an trial-and-error basis (Pilkington, 2009). The smaller the compacting parameter σ, the more focused the model will be. After the first step, the DEXP transformation of the difference between the measured and predicted data is computed, and then the model correction is evaluated by converting Ω into the physical property (Equation 5). Therefore, the model at the ith step will be given by

$$\rho_i = \rho_{i-1} + k_i \mathbf{W}_{i-1} \mathbf{A} \Omega_{dif} \tag{7}$$

and accordingly, the field will be calculated as

$$\mathbf{d}_i^{\text{cal}} = \mathbf{A}\rho_i \tag{8}$$

where $\mathbf{A}$ is the kernel matrix, $\mathbf{\Omega}_{\text{dif}}$ is the DEXP of data misfit and k_i is the converting constant, calculated by performing a linear regression of the data misfit versus the field predicted from the DEXP transformation of data misfit at the iteration $(i-1)$ with a unit density or magnetization.

Thus,

$$\mathbf{d}^{\text{obs}} - \mathbf{d}_{i-1}{}^{\text{cal}} = k_i \mathbf{A} \mathbf{\Omega}_{\text{dif}} \tag{9}$$

Then the compacting function is updated based on Equation 6, and the iteration continues until the RMS value of data misfit changes slightly.

5. Imaging Results

In the following section, we illustrate the iterative CDEXP imaging of seven diapirs of the Nordkapp Basin. We first reduced to the pole the filtered field of Figure 1c assuming an induced-only magnetization (inducing field inclination = 79.5° and declination = −19.3°), then we upward continued the data to a maximum altitude of 5,000 m a.s.l. with a continuation step of 100 m. Finally, we computed the second vertical derivative of the pole-reduced continued field and performed our iterative compacting DEXP transformation on a subarea of the investigated data set (Figure 3).

We used the compacting factor $\sigma = 0.1$, and $N = 0.6$, the mean range value found by the scaling function analysis (see Figure 2). Also, we constrained the lower and upper bounds of the magnetization contrast to −0.2–0 A/m.

The recovered model obtained by imaging after 70 iterations is shown in Figure 3. The investigated volume in the underground reaches 5,000 m depth. The 3-D model highlights the position and extent of the seven investigated diapirs. Their maximum magnetization contrast is −0.08 A/m, which agrees with the most probable contrast between sedimentary layers and salt diapirs (Lauritsen et al., 2007; Mørk et al., 2002). Their depth ranges from about 500 m b.s.l. (that is, their top is close to the sea bottom), to about 4,000 m b.s.l. Diapirs # 1, 2, and 4 ("Uranus"; Stadtler et al., 2014) are the deepest ones and extend down to 3,500–4,000 m b.s.l. Diapirs # 6 and # 7 ("G2" and "F2", respectively, in Tu & Zhdanov, 2020 and Xu et al., 2020) reach 2000 m b.s.l., whereas diapirs #3 and #5 are the shallowest ones, with #5 not exceeding 1,500 m depth and having the weakest magnetization contrast. A comparison between the input and predicted data from CDEXP imaging (Figures 3c–3e) shows that the fitting is rather good.

6. Discussion

Potential field problems are ill-posed, and therefore inherently difficult to solve. Specifically, they fail to have a unique solution, and the solution may be extremely sensitive to errors. These difficulties are due to certain kinds of ambiguities such as the inherent, algebraic and error ambiguity (Fedi et al., 2005; Paoletti et al., 2014). These kinds of ambiguity may lead to a loss of depth information and add to the problem of obtaining reliable information about the source distribution. In this paper we reduce the inherent ambiguity of magnetic data imaging by incorporating a priori information in the form of magnetization lower and upper bounds and of a compacting factor leading to focused solutions.

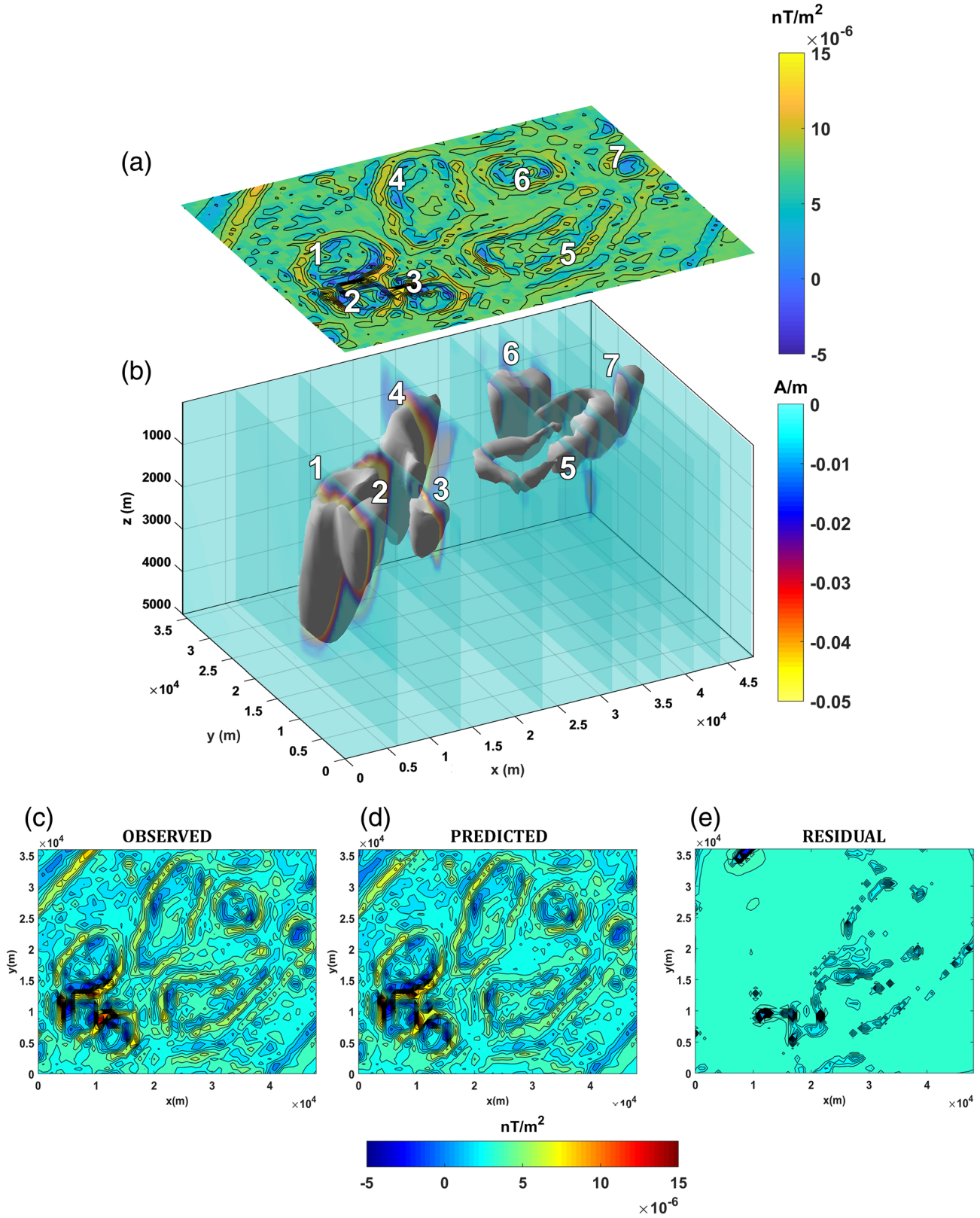

Figure 3. Imaging results for the seven analyzed diapirs in the Nordkapp Basin: (a) Second-order vertical derivative of the pole-reduced data, considered in our imaging; white numbers point out the seven studied diapirs; (b) results from the compact DEXP. The isosurface is relative to a contrast of −0.05 a/m; (c) second-order vertical derivative of the pole-reduced data; (d) predicted data by the CDEXP imaged model of plot (b); (e) data misfit.

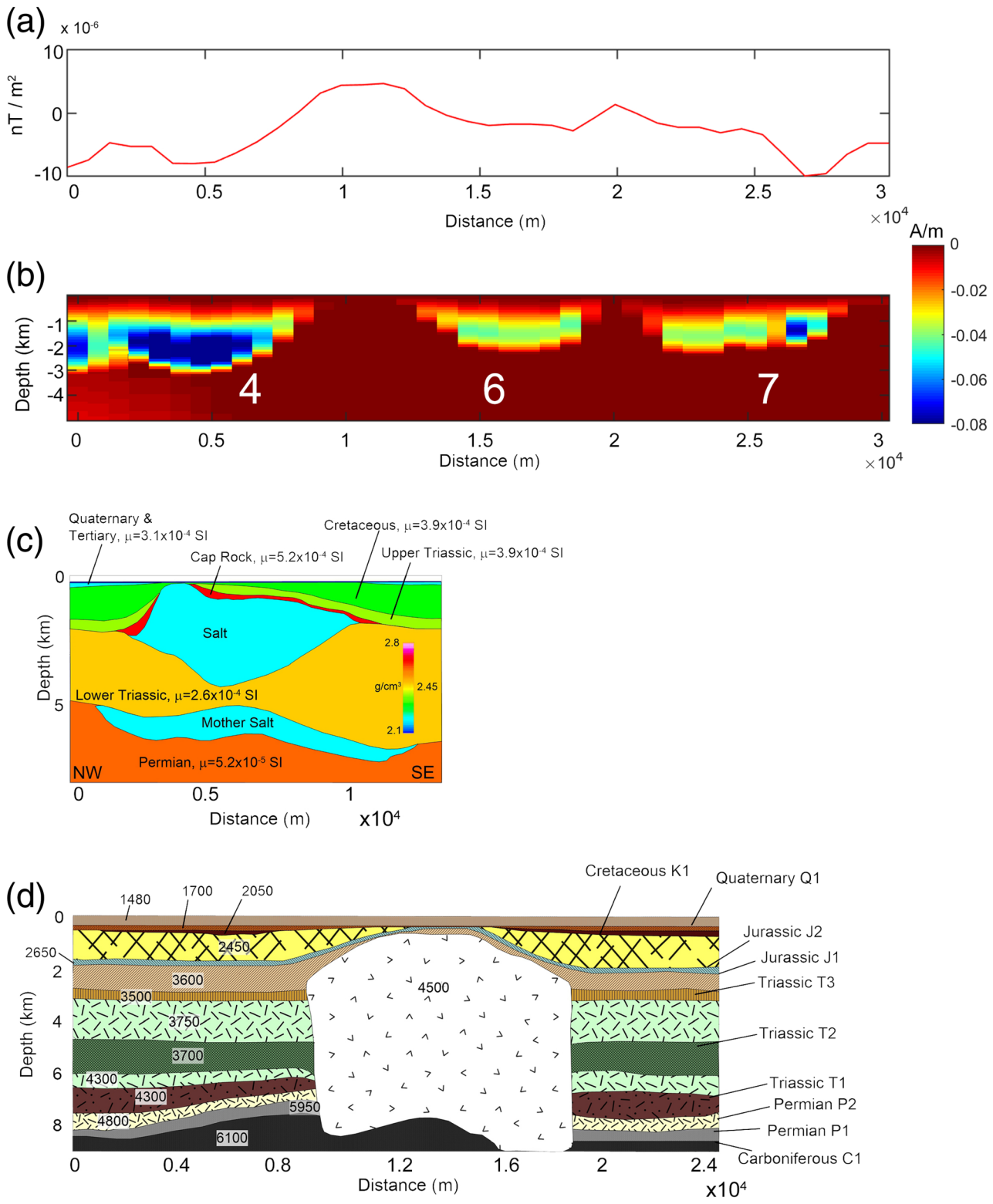

Figure 4. Comparison among geophysical models at Nordkapp: (a) Data along profile P2 (see Figure 2a for location of the profile); (b) results of our 3-D imaging along P2, crossing diapirs Uranus (# 4), G2 (# 6), and F2 (# 7); (c) density and magnetic susceptibility model for Uranus (modified after Stadtler et al., 2014); (d) seismic data interpretation of the typical diapirs of the Nordkapp basin (modified after Koyi et al., 1993; the numbers to the left are the velocities of the different layers in m/s).

Multiscale methods have shown to be useful to achieve detailed information in the framework of the Nordkapp diapirs. These saline structures are diamagnetic and are characterized by a negative magnetization contrast with respect to the surrounding Cretaceous layers (in which a quantity of magnetic minerals is found). The resulting 3-D model of seven diapirs of the area shows that they extend from 500 m to 4,000 m b.s.l. and are characterized by a general low-magnetization contrast, not larger than −0.08 A/m (about $1{,}900 \times 10^{-6}$ SI units), that is well in agreement with the range of induced magnetizations found by studies of the magnetic properties of stratigraphic cores (Lauritsen et al., 2007; Mørk et al., 2002; Stadtler et al., 2014). We remark that as we have a magnetization contrast varying versus depth (Stadtler et al., 2014), our solution provides an average magnetization contrast, also called *effective contrast* (Chauhan et al., 2018; Litinsky, 1989). The found source depths agree with 2-D seismic reflection sections and potential field modeling (Gernigon et al., 2014). More specifically, the depths retrieved for diapirs #1–3 and 4 and 5 match with the studies by Nilsen et al. (1995), who inferred values for the two-way traveltime ranging from 0.5 s and to about 3 s, with the diapir # 4 deeper than # 5. Our results also agree with 2-D seismic reflection sections on diapirs # 5 and 7 performed by Rojo and Escalona (2018). The authors found values for the two-way traveltime ranging from 0.5 s and to about 1.6 s for the shallowest Diapir # 5 and ranging from 0.5 s and to about 3 s for diapir # 7.

A profile through our 3-D model along diapirs Uranus, G2, and F2 (#4, 6, and 7, respectively; Figure 4) highlights a fairly good agreement between our results and a previous 2-D density and magnetic susceptibility model of Diapir # 4 ("Uranus") (Stadtler et al., 2014). Also, the depths inferred by our 3-D model agree with the interpretation results of 2-D seismic reflection profiles (Koyi et al., 1993). Finally, our results fairly agree with the salt structures of basin imaged by Tu and Zhdanov (2020), Wan and Zhdanov (2008), and Xu et al. (2020) from gravity gradiometry data.

7. Concluding Remarks

Defining the salt domes geometry and depth is of great economic interest as these structures can act as traps for hydrocarbons. However, these features are not always hypothesized by conventional geophysical methods. For example, gravimetric data can fail where the density contrast between the saline structures and the surrounding sediments are negligible. Seismic methods, on the other hand, may not be effective due to imaging distortion around the salt diapir which lead to difficulties in the mapping of the salt base. In this study we provide a new perspective of salt-dome exploration by means of multiscale magnetic field analysis. The results show that imaging methods employed on high-resolution magnetic data can well-identify the saline structures top, bottom, and shape thanks to the, albeit small, contrast of magnetization of the tilted and/or folded layers with respect to the diamagnetic salt. Thus, we believe that the multiscale analysis of magnetic field data may represent a valid tool to provide a picture of salt domes and characterize their features especially when other methods are not entirely effective.

Data Availability Statement

Geophysical data of the Barents Sea region are open and available by request at NGU and NPD websites (https://www.ngu.no/en, https://www.npd.no/en/).

Acknowledgments
The authors acknowledge Christine Fichler, the Norwegian Survey of Geology and Statoil for data availability and permission. The authors are grateful to the reviewers Michael Zhdanov and Fabio Caratori Tontini for their constructive comments that helped in improving our manuscript. The authors thank Rosa Mariarca Di Somma for preliminary computations and David Giampietro for language revision.

References

Backé, G., Baines, G., Giles, D., Preiss, W., & Alesci, A. (2010). Basin geometry and salt diapirs in the Flinders ranges, South Australia: Insights gained from geologically-constrained modelling of potential field data. *Marine and Petroleum Geology*, *27*(3), 650–665. https://doi.org/10.1016/j.marpetgeo.2009.09.001

Bain, J., Horscroft, T. R., Weyand, J., Saad, A. H., & Bulling, D. N. (1993). Complex salt features resolved by integrating seismic, gravity and magnetics: European Association of Petroleum Geophysicists (EAGP)/European Association of Exploration Geophysicists (EAEG), 55th Conference and Technical Exhibition, 8 June 1993, Stavanger, Norway, Abstracts, no. E006, doi: https://doi.org/10.3997/2214-4609.201411696. pp. 1–4.

Baniamerian, J., Fedi, M., & Oskooi, B. (2016). Research note: Compact depth from extreme points: A tool for fast potential field imaging. *Geophysical Prospecting*, *64*(5), 1386–1398. https://doi.org/10.1111/1365-2478.12365

Baniamerian, J., Oskooi, B., & Fedi, M. (2017). Source imaging of potential fields through a matrix space-domain algorithm. *Journal of Applied Geophysics*, *136*, 51–60. https://doi.org/10.1016/j.jappgeo.2016.10.035

Barde, J. P., Chamberlain, P., Galavazi, M., Harwijanto, J., Marsky, J., Gralla, P., & van den Belt, F. (2002). Sedimentation during halokinesis: Permo-Triassic reservoirs of the Saigak field, Precaspian Basin, Kazakhstan. *Petroleum Geoscience*, *8*(2), 177–187. https://doi.org/10.1144/petgeo.8.2.177

Bugge, T., Elvebakk, G., Fanavoll, S., Mangerud, G., Smelror, M., Weiss, H. M., et al. (2002). Shallow stratigraphic drilling applied in hydrocarbon exploration of the Nordkapp Basin, Barents Sea. *Marine and Petroleum Geology*, *19*(1), 13–37. https://doi.org/10.1016/S0264-8172(01)00051-4

Chauhan, M. S., Fedi, M., & Senn, M. K. (2018). Gravity inversion by the multi-homogeneity depth estimation method for investigating salt domes and complex sources. *Geophysical Prospecting*, *66*(S1), 175–191. https://doi.org/10.1111/1365-2478.12603

Choi, S., Gtze, H.-J., Meyer, U., & Desire Group (2011). 3-D density modeling of underground structures and spatial distribution of salt diapirism in the Dead Sea Basin. *Geophysical Journal International*, *184*(3), 1131–1146. https://doi.org/10.1111/j.1365-246X.2011.04939.x

Davison, I., Alsop, G. I., Evans, N. G., & Safaricz, M. (2000). Overburden deformation patterns and mechanisms of salt diapir penetration in the central Graben, North Sea. *Marine and Petroleum Geology*, *17*(5), 601–618. https://doi.org/10.1016/S0264-8172(00)00011-8

Faleide, J. I., Gudlauqsson, S. T., & Jacquart, G. (1984). Evolution of the western Barents Sea. *Marine and Petroleum Geology*, *1*(2), 123–150. https://doi.org/10.1016/0264-8172(84)90082-5

Fedi, M. (2007). DEXP: A fast method to determine the depth and the structural index of potential fields sources. *Geophysics*, *72*(1), I1–I11. https://doi.org/10.1190/1.2399452

Fedi, M., Cella, F., D'Antonio, M., Florio, G., Paoletti, V., & Morra, V. (2018). Gravity modeling finds a large magma body in the deep crust below the Gulf of Naples, Italy. *Scientific Reports*, *8*, 8229. https://doi.org/10.1038/s41598-018-26346-z

Fedi, M., Cella, F., Quarta, T., & Villani, A. (2010). 2D continuous wavelet transform of potential fields due to extended source distributions. *Applied and Computational Harmonic Analysis*, *28*(3), 320–337. https://doi.org/10.1016/j.acha.2010.03.002

Fedi, M., & Florio, G. (2001). Detection of potential fields source boundaries by enhanced horizontal derivative method. *Geophysical Prospecting*, *49*(1), 40–58. https://doi.org/10.1046/j.1365-2478.2001.00235.x

Fedi, M., Florio, G., & Cascone, L. (2012). Multiscale analysis of potential fields by a ridge consistency criterion: The reconstruction of the bishop basement. *Geophysical Journal International*, *188*(1), 103–114. https://doi.org/10.1111/j.1365-246X.2011.05259.x

Fedi, M., Florio, G., & Paoletti, V. (2015). MHODE: A local-homogeneity theory for improved source-parameter estimation of potential fields. *Geophysical Journal International*, *202*(2), 887–900. https://doi.org/10.1093/gji/ggv185

Fedi, M., Florio, G., & Quarta, T. (2009). Multiridge analysis of potential fields: Geometrical method and reduced Euler deconvolution. *Geophysics*, *74*(4), L53–L65. https://doi.org/10.1190/1.3142722

Fedi, M., Hansen, P. C., & Paoletti, V. (2005). Tutorial: Analysis of depth resolution in potential field inversion. *Geophysics*, *70*(6), A1–A11. https://doi.org/10.1190/1.2122408

Fedi, M., & Pilkington, M. (2012). Understanding imaging methods for potential field data. *Geophysics*, *77*(1), G13–G24. https://doi.org/10.1190/geo2011-0078.1

Fichler, C., Rueslåtten, H., Gram, C., Ingebrigtsen, A., & Olesen, O. (2007). Salt interpretation with special focus on magnetic data, Nordkapp Basin, Barents Sea: 2007 International workshop *Innovation in EM, Grav and Mag Methods (EGM 2007): A new perspective for exploration*. Capri, Italy, extended abstract: http://earthdoc.org/detail.php?pubid=39235

Florio, G., Fedi, M., & Rapolla, A. (2009). Interpretation of regional aeromagnetic data by the scaling function method: The case of Southern Apennines (Italy). *Geophysical Prospecting*, *57*(4), 479–489. https://doi.org/10.1111/j.1365-2478.2009.00807.x

Gabrielsen, R. H., Færseth, R. B., Jensen, L. N., Kalheim, J. E., & Riis, F. (1990). Structural elements of the Norvegian continental shelf—Part 1: The Barents Sea region. *Norwergian Petroleum Directorate (NPD) Bulletin*, *6*, 33.

Geletti, R., Zgur, F., Del Ben, A., Buriola, F., Fais, S., Fedi, M., et al. (2014). The Messinian salinity crisis: New seismic evidence in the West-Sardinian margin and Eastern Sardo-Provençal basin (West Mediterranean Sea). *Marine Geology*, *351*, 76–90. https://doi.org/10.1016/j.margeo.2014.03.019

George, M., Olakunle, O. K., Emil, J. S., & Abrahamson, P. (2017). Seismic interpretation and characterization of anhydrite caprocks in the Tromso Basin, SW Barents Sea. *Marine Geology*, *390*, 36–50. https://doi.org/10.1016/j.margeo.2017.04.013

Gernigon, L., Bronner, M., Fichler, C., Lovas, L., Marello, L., & Olesen, O. (2011). Magnetic expression of salt diapir-related structures in the Nordkapp Basin, western Barents Sea. *Geology*, *39*(2), 135–138. https://doi.org/10.1130/G31431.1

Gernigon, L., Brönner, M., Roberts, D., Olesen, O., Nasuti, A., & Yamasaki, T. (2014). Crustal and basin evolution of the southwestern Barents Sea: From Caledonian orogeny to continental breakup: Evolution of the Barents Sea. *Tectonics*, *33*, 347–373. https://doi.org/10.1002/2013TC003439

Gudlaugsson, S. T., Faleide, J. I., Johansen, S. E., & Breivik, A. J. (1998). Late Palaeozoic structural development of the South-Western Barents Sea. *Marine and Petroleum Geology*, *15*(1), 73–102. https://doi.org/10.1016/S0264-8172(97)00048-2

Hayward, N., Dehler, S. A., Grant, A. C., & Durling, P. (2014). Magnetic anomalies associated with salt tectonism, deep structure and regional tectonics in the Maritimes Basin, Atlantic Canada. *EAGE Basin Research*, *26*(2), 320–337. https://doi.org/10.1111/bre.12029

Henriksen, S., & Vorren, T. O. (1996). Early tertiary sedimentation and salt tectonics in the Nordkapp Basin, southern Barents Sea. *Norsk Geologisk Tidsskrift*, *76*, 33–44.

Johansen, S. E., Ostisty, B. K., Birkeland, Ø., Fedorovsky, Y. F., Martirosjan, V. N., Bruun, C. O., et al. (1992). Hydrocarbon potential in the Barents Sea region: Play distribution and potential. *Norwegian Petroleum Society Special Publications*, *2*, 273–320.

Koehl, J. B. P., Bergh, S. G., Henningsen, T., & Faleide, J. I. (2018). Middle to late Devonian-carboniferous collapse basins on the Finnmark platform and in the southwesternmost Nordkapp basin, SW Barents Sea. *Solid Earth*, *9*(2), 341–372. https://doi.org/10.5194/se-9-341-2018

Koyi, H., Talbot, C. J., & Tørudbakken, B. O. (1993). Salt diapirs of the southwest Nordkapp Basin: Analogue modelling. *Tectonophysics*, *228*(3-4), 167–187. https://doi.org/10.1016/0040-1951(93)90339-L

Lauritsen, T., Blomstrand, L.B., Olesen, O., & Mørk, A. (2007). OSRAM II—Origin of sediment-related AeroMagnetics II: Magnetic susceptibility measurements on shallow stratigraphic cores from the Finnmark platform, Nordkapp Basin and Svalis Dome: Trondheim, Geological Survey of Norway (NGU), report 2007.028, 109 pp.

Litinsky, V. (1989). Concept of effective density: Key to gravity depth determinations for sedimentary basins. *Geophysics*, *54*(11), 1474–1482. https://doi.org/10.1190/1.1442611

Liu, S., Baniamerian, J., & Fedi, M. (2020). Imaging methods versus inversion methods. An option or an alternative? *IEEE Transactions on Geoscience and Remote Sensing*, *58*(5), 3484–3494. https://doi.org/10.1109/TGRS.2019.2957412

Mastellone, D., Fedi, M., Ialongo, S., & Paoletti, V. (2014). Volume upward continuation of potential fields from the minimum-length solution: An optimal tool for continuation through general surfaces. *Journal of Applied Geophysics*, *111*, 346–355. https://doi.org/10.1016/j.jappgeo.2014.10.020

Mattos, N. H., Alves, T. M., & Omosanya, K. O. (2016). Crestal fault geometries reveal late halokinesis and collapse of the Samson dome, northern Norway: Implications for petroleum systems in the Barents Sea. *Tectonophysics*, *690*, 76–96. https://doi.org/10.1016/j.tecto.2016.04.043

Milano, M., Fedi, M., & Fairhead, J. D. (2016). The deep crust beneath the Trans-European Suture Zone from a multiscale magnetic model. *Journal of Geophysical Research: Solid Earth*, *121*, 6276–6292. https://doi.org/10.1002/2016JB012955

Mørk, M. B. E., McEnroe, S. A., & Olesen, O. (2002). Magnetic susceptibilities of Mesozoic and Cenozoic sediments off mid Norway and the role of siderite: Implications for interpretation of high-resolution aeromagnetic anomalies. *Marine and Petroleum Geology*, *19*(9), 1115–1126. https://doi.org/10.1016/S0264-8172(02)00115-0

Nabighian, M. N., Grauch, V. J. S., Hansen, R. O., LaFehr, T. R., Li, Y., Peirce, J. W., et al. (2005). 75th anniversary—The historical development of the magnetic method in exploration. *Geophysics*, *70*(6), 33–61. https://doi.org/10.1190/1.2133784

Nilsen, K. T., Vendeville, B. C., & Johansen, J. T. (1995). Influence of regional tectonics on halokinesis in the Nordkapp Basin, Barents Sea. In M. P. A. Jackson, D. G. Robert, & S. Snelson (Eds.), *Salt tectonics: A global perspective*, *Memoir* (Vol. 65, pp. 413–436). Tulsa, OK: American Association of Petroleum Geologists (AAPG).

Olesen, O., Brönner, M., Ebbing, J., Gellein, J., Gernigon, L., Koziel, J., et al. (2010). New aeromagnetic and gravity compilations from Norway and adjacent areas: Methods and applications. *Petroleum Geology Conference Series*, *7*(1), 559–586. https://doi.org/10.1144/0070559

Paoletti, V., Buggi, A., & Pasteka, R. (2019). UXO detection by multiscale potential field methods. *PAGEOPH-Pure and Applied Geophysics*, *176*(10), 4363–4381. https://doi.org/10.1007/s00024-019-02202-7

Paoletti, V., Hansen, P. C., Hansen, M. F., & Fedi, M. (2014). A computationally efficient tool for assessing the depth resolution in potential-field inversion. *Geophysics*, *79*(4), A33–A38. https://doi.org/10.1190/GEO2014-0017.1

Paoletti, V., Passaro, S., Fedi, M., Marino, C., Tamburrino, S., & Ventura, G. (2016). Sub-circular conduits and dikes offshore the Somma-Vesuvius volcano revealed by magnetic and seismic data. *Geophysical Research Letters*, *43*, 9544–9551. https://doi.org/10.1002/2016GL070271

Pilkington, M. (2009). 3D magnetic data-space inversion with sparseness constraints. *Geophysics*, *74*(1), L7–L15. https://doi.org/10.1190/1.3026538

Rojo, L. A., & Escalona, A. (2018). Controls on minibasin infill in the Nordkapp Basin: Evidence of complex Triassic synsedimentary deposition influenced by salt tectonics. *AAPG Bulletin*, *102*(07), 1239–1272. https://doi.org/10.1306/0926171524316523

Rønnevik, H. C., & Jacobsen, H. P. (1984). Structural highs and basins in the western Barents Sea. In A. M. Spencer, E. Holter, S. O. Johnsen, A. Mørk, E. Nysaether, P. Songstad, & Å. Spinnangr (Eds.), *Petroleum geology of the Northwest European Margin*, *Norwegian Petroleum Society (NPF)* (pp. 19–32). London: Graham & Trotman.

Rowan, M. G., & Vedenville, B. C. (2006). Foldbelts with early salt withdrawal and diapirism: Physical model and examples from the northern Gulf of Mexico and the Flinders ranges, Australia. *Marine and Petroleum Geology*, *23*(9-10), 871–891. https://doi.org/10.1016/j.marpetgeo.2006.08.003

Saad, A. H. (1993). Interactive integrated interpretation of gravity, magnetic, and seismic data—Tools and examples: Offshore Tech. Conf. Proceedings, Paper OTC-7079, 35–44.

Stadtler, C., Fichler, C., Hokstad, K., Myrlund, E. A., Wienecke, S., & Fotland, B. (2014). Improved salt imaging in a basin context by high resolution potential field data: Nordkapp Basin, Barents Sea. *Geophysical Prospecting*, *62*(3), 615–630. https://doi.org/10.1111/1365-2478.12101

Tu, X., & Zhdanov, M. (2020). Enhancement and sharpening the migration images of the gravity field and its gradients. *Pure and Applied Geophysics*, *177*(6), 2853–2870. https://doi.org/10.1007/s00024-019-02397-9

Vorren, T. O., Richardsen, G., Knutsen, S.-M., & Henriksen, E. (1991). Cenozoic erosion and sedimentation in the western Barents Sea. *Marine and Petroleum Geology*, *8*(3), 317–340. https://doi.org/10.1016/0264-8172(91)90086-G

Wan, L., & Zhdanov, M. S. (2008). Focusing inversion of marine full-tensor gradiometry data in offshore geophysical exploration. In *78th SEG Technical Program Expanded Abstracts 2008* (pp. 751–754). Tulsa, OK: Society of Exploration Geophysicists. https://doi.org/10.1190/1.3063755

Xu, Z., Wan, L., & Zhdanov, M. (2020). Focusing iterative migration of gravity gradiometry data acquired in Nordkapp basin, Barents Sea. Geophysical Prospecting, First published: 11 June 2020, https://doi.org/10.1111/1365-2478.12990